

Turbulence collapses at a threshold particle loading in a dilute particle-gas suspension

V. KUMARAN¹, N. S. P. MURAMULLA², A. TYAGI¹ and P. S. GOSWAMI²

¹ Department of Chemical Engineering, Indian Institute of Science - Bangalore 560 012, India

² Department of Chemical Engineering, Indian Institute of Technology Bombay - Mumbai 400 076, India

received 19 August 2019; accepted in final form 20 December 2019

published online 6 February 2020

PACS 47.55.Kf – Particle-laden flows.

PACS 47.27.E- – Turbulence simulation and modeling.

Abstract – Direct Numerical Simulations (DNS) of the flow of a particle-gas suspension in a channel have been carried out to examine the turbulence attenuation due to particles. As the volume fraction is increased in the range $0-3.5 \times 10^{-3}$, there is a discontinuous decrease in the turbulent velocity fluctuations at a critical volume fraction. The turbulent energy production rate decreases by an order of magnitude, accompanied by a much smaller increase in the energy dissipation due to particle drag, resulting in a decrease in the total energy dissipation. In contrast to the current understanding, the results show that turbulence attenuation is a discontinuous process, and is due to a disruption of the turbulent energy production mechanism, and not due to the increased dissipation due to the particles.

Copyright © EPLA, 2020

Introduction. – A central issue in the dynamics of turbulent particle-gas suspensions is the effect of the particles on the gas phase turbulence. The turbulent velocity fluctuations transport and redistribute particles across the flow, and could cause enhanced aerosol dispersion, drop coalescence as well as the break-up of large drops. An important question, which has been studied extensively, is whether the fluid turbulence is increased or decreased due to the presence of the particles. Large particles could enhance the turbulent fluctuations due to the wake generated behind the particles, while small particles are known to attenuate turbulence due to particle drag. The effect of particles is an additional layer of complexity on the already complex problem of turbulent flows; however, it is also critical for predicting the fate of important natural processes such as aerosol transport, formation of rain drops and snow flakes, the phenomena such as sand and dust storms, and in the modeling of important industrial processes such as fluidised/circulating beds and pneumatic transport of fine particles.

The appropriate drag law depends on the particle Reynolds number (ratio of the fluid inertia and viscosity at the particle scale) based on the relative velocity between the fluid and particles, the particle diameter and gas viscosity. If terminal velocity is considered as the relative velocity scale, the particle Reynolds number is $(\rho_p \rho_f g d_p^3 / 18 \mu^2)$, where ρ_p and ρ_f are the particle and

fluid density, g is the acceleration due to gravity, d_p is the particle diameter and μ is the fluid viscosity. When particles of diameter $100 \mu\text{m}$ or less and mass density of about 2000 kg m^{-3} , are suspended in air with density 1.2 kg m^{-3} and viscosity $1.8 \times 10^{-5} \text{ kg m}^{-1} \text{ s}^{-1}$, the particle Reynolds number is less than 8.5. Due to the small Reynolds number, the drag force on the particles can be adequately described by the Stokes law or a modified drag law that incorporates inertial corrections. The particle Stokes number (ratio of particle inertia to fluid viscosity) is typically large, about $O(10^3)$ higher than the particle Reynolds number due to the large ratio of particle and gas densities. Due to this, the particles cross the fluid streamlines due to inertia, and there is a force exerted on the fluid due to the instantaneous difference in the particle and fluid velocities.

It is reported in an early review [1] that the turbulence modification is determined by the ratio (d_p/L) , where d_p is the particle diameter and L is the integral length scale of turbulence. Turbulence was found to be suppressed for $(d_p/L) < 0.1$, and augmented for $(d_p/L) > 0.1$. Direct Numerical Simulations (DNS) of particle-laden turbulent flows have predicted that the particles are preferentially concentrated in high strain regions, and expelled from high vorticity regions [2]. It was also observed that particles increase the turbulent energy at high wave numbers. A transfer of energy from the large to small scales in the

absence of gravity, and a reverse cascade from small to large scales in the presence of gravity was reported [3]. In particle-laden vertical channel flow, Li and McLaughlin [4], reported that particles increase turbulence at low mass loading of 0.2, but the particles could attenuate turbulence by up to 90% at a higher mass loading of 2. Based on a review of experimental and numerical results, a particle momentum number was identified [5]. It was found that particles with small momentum number increase turbulence, whereas those with moderate momentum number decrease turbulence. Recent simulations [6,7] report that the turbulence intensity progressively decreases with particle loading, as the increased dissipation due to the particles compensates for the decrease in the fluid turbulent energy production. The generation of particle-induced fluctuations due to clustering of the particles has also been investigated [8]. Based on previous studies [7,8], the consensus is that there is a gradual decrease in the turbulence intensities with increasing particle loading, and this gradual decrease is caused by the increasing dissipation of energy due to the particles. The range of Reynolds number, Stokes number and particle volume fraction examined in previous studies is as follows. The fluid Reynolds number (based on the characteristic flow scale and the flow velocity) reported in references [4,9,10] usually varies in the range of 3000 to 5600, though Reynolds numbers greater than 10000 have also been used in few studies [6,7]. In simulations where the flow around the particles is not resolved, the particle Reynolds number is less than 100 and Stokes number is less than 30. The particle mass loading used in the earlier studies varies between 0 to 20 [4,6,7].

Here, we critically examine the turbulence attenuation mechanism, specifically whether the decrease in turbulence intensity is continuous as the particle loading is increased, and whether the excess dissipation due to the particle phase does result in turbulence attenuation. Since the objective of the present study is to detect changes in the turbulence attenuation due to the particle loading, a large number of simulations were required at different particle volume fractions and at different particle Stokes numbers.

Two different values of the channel Reynolds number based on the mean flow velocity \bar{u} and channel width h , $Re = (\bar{u}h/\nu) = 3300$ and 5600 , both in the turbulent regime, have been used. The equivalent Reynolds numbers $Re_{max} = (u_{max}h/2\nu)$ based on the half channel width ($h/2$), and the maximum velocity (u_{max}) are 2000 and 3360 respectively. The friction Reynolds number $Re_* = (u_*h/2\nu)$, based on the friction velocity u_* are 115 and 180 respectively. For comparison, the transition to turbulence in a channel flow takes place in the range $975 \lesssim Re_{max} \lesssim 1200$, $1300 \lesssim Re \lesssim 1800$ and $62.5 \lesssim Re_* \lesssim 73.5$ [11–13]. Thus the Reynolds numbers Re used here are 1.8 and 3 times the upper end of the transitional regime, and the flow is fully turbulent. For the unladen flow, the Kolmogorov length scale, $\eta = (\nu^3/\epsilon)^{1/4}$, is about 0.7×10^{-2} times the channel width near the wall

and 1.6×10^{-2} times the channel width at the center. Here ϵ is the rate of dissipation of energy due to the turbulent fluctuations at the wall, and $\nu = (\mu/\rho)$ is the kinematic viscosity.

The relevant velocity for the flow around a particle is the local difference between the particle and fluid velocities, which is about 5–8 times smaller than the average flow velocity. The particle Reynolds number $Re = (d_p \Delta u / \nu)$, based on the particle diameter d_p and the root mean square of the velocity difference between the particles and fluid Δu is in the range 4–15 for all the Reynolds and Stokes numbers reported here. Since the particle Reynolds number is greater than 1, the Stokes drag law cannot be used. An inertia corrected drag law [14],

$$\mathbf{F}_I^D = 3\pi\mu d_p(\mathbf{u} - \mathbf{v}_I)(1 + 0.15Re_I^{0.687}), \quad (1)$$

is used. Here, \mathbf{F}_I^D is the drag force on particle I , \mathbf{v}_I is the particle velocity, \mathbf{u} is the fluid velocity at the particle location, d_p is the particle diameter, and Re_I is the particle Reynolds number based on the particle diameter, difference in gas and particle velocities $|\mathbf{u} - \mathbf{v}_I|$ and the gas kinematic viscosity. Equation (1) is accurate to within about 0.2% when the particle Reynolds number Re_p is less than 15.

The particle Stokes number is the ratio of the viscous relaxation time and the fluid integral time scale. The latter here has been considered as $\tau_f = (h/\bar{u})$. For the inertia corrected drag law (eq. (1)), the viscous relaxation time is $\tau_v = (\rho_p d_p^2 / 18\mu(1 + 0.15Re^{0.687}))$. The ratio of the two time scales, $St = (\tau_v/\tau_f)$ is varied in the range 1.62–130 when the channel Reynolds number is 3300, and 25–75 when the Reynolds number is 5600.

The time scale based on the friction velocity and kinematic viscosity is $\tau_{f*} = (\nu/u_*^2)$, and the Stokes number based on the friction velocity is defined as $St_* = (\tau_v/\tau_{f*})$. The ratio of the Stokes number based on friction velocity and that based on the integral scale, $(St_*/St) = (\tau_f/\tau_{f*})$, can be expressed in terms of the channel and friction Reynolds numbers as $4Re_*^2/Re$. This ratio is about 16 for $Re = 3300$ and about 23 for $Re = 5600$. Since the present study is related to particles whose viscous relaxation time is much larger than the flow time scales, these particles interact with fluid structures having largest time scale in the turbulent flow, which is the integral time scale for fluid turbulence. Therefore, we have defined the Stokes number based on the integral time scale in this study.

The particles are considered to be rigid spheres, and the ratio of the particle diameter and the channel width is 1.84×10^{-2} . The particle terminal velocity is 4×10^{-3} smaller than the fluid average velocity, and so the gravitational force on the particles is negligible compared to the drag force due to the fluid. The ratio of the particle and fluid densities, (ρ_p/ρ_f) is equal to $(18St/Re)(h/d_p)^2$, where the Stokes number is $(\rho_p d_p^2 \bar{u} / 18\mu h)$ and the Reynolds number is $(\rho_f \bar{u} h / \mu)$. For the present simulations, the ratio of mass densities is $16.4St$ for $Re = 3300$, and $9.5St$ for $Re = 5600$. Here, (ρ_p/ρ_f) has been varied

over the range 330–6667 for $Re = 3300$ and in the range 500–3000 for $Re = 5600$. For a volume fraction 2×10^{-3} , the mass loading $(\rho_p/\rho_f)\phi$ is in the range 0.66–13.3 for $Re = 3300$, and in the range 1–6 for $Re = 5600$.

Recent studies [15,16] have pointed out that the point-particle approximation is valid if the ratio of the particle relaxation time and the Kolmogorov time is large, even when the particle diameter and Kolmogorov scale are comparable. The Stokes number based on the Kolmogorov time is defined as $St_k \approx (\rho_p/18\rho_f)(d_p/\eta)^2$, where η is the Kolmogorov scale. A comparison of particle-resolved and point-particle simulations [17] has found that there is excellent agreement in the results for the kinetic energy and energy dissipation rates for $(d/\eta) = 1$ when $St_k = 100$, provided the correction for the undisturbed velocity at the particle center (discussed in the section “Particle force laws”) is incorporated. In the present study, the particle diameter is comparable to the Kolmogorov scale, but the ratio $(\rho_p/18\rho_f) \sim O(10^2)$. Therefore, we have used the point-particle approximation, along with the velocity correction algorithm [18] to obtain the undisturbed velocity field used in drag force calculation.

The particle volume fraction, in the range $0\text{--}3.5 \times 10^{-3}$, is at the higher end of the range of volume fractions used in earlier studies. The values of the particle Reynolds number (4–15) are comparable to those used in previous studies. However, the range of particle Stokes numbers used here, in the range 0–130, is significantly higher than those used in previous investigations. In this range of parameters, we find a new phenomenon, which is the discontinuous decrease in the turbulence intensities as the particle volume fraction is increased.

Particle force laws. – Care has to be exercised in modeling the drag force on the particles, since there are numerous physical effects which could affect the drag force. Since the volume fraction of the particles is, at most, 3.5×10^{-3} , simultaneous multi-particle interactions are neglected in comparison to binary collisions between pairs of particles. However, there are several single-particle effects which could affect the drag force. In the low Reynolds number limit, the drag force depends on the “undisturbed” velocity at the particle center, that is, the far-field velocity in the absence of the particle. Simulations [17,18] have shown that it is necessary to correct for the undisturbed velocity even at moderate particle Reynolds number in order to correctly capture the drag force in particle-resolved simulations. There is also a particle lift force [19–21] due to inertial effects in a shear flow or when a particle is translating relative to the fluid. There are also corrections to the drag and lift forces due to the presence of a nearby wall [22]. While the effect of inertia and boundaries on the drag and lift forces have been studied for some time now, there is still a lot more work to be done for refining the expressions of the force and extending their validity, as well as for refining the torque on a particle due to inertia and wall effects.

As explained previously, the objective here is to study the qualitative features of turbulence modification due to the presence of particles. In particular, we are interested in examining if the turbulence intensity decreases continuously as the particle volume fraction increases, and whether the turbulence attenuation is due to an increase in the dissipation of energy due to particle drag. Rather than carrying out simulations for one specific particle force model which is subject to revision due to further research, we have also examined the dependence of the qualitative features and quantitative measures of turbulence modification on the force law.

Apart from the results shown here using eq. (1) for the drag force on a particle, simulations have also been performed using the correction for the “undisturbed” velocity using the procedure of [18], the particle lift force using the expression of [21] and the wall corrections to the drag and lift forces proposed in [22]. When the correction due to undisturbed velocity field is included, there is a decrease of about 10% in the mean square velocities, but virtually no change when the lift force and the wall corrections to the drag and lift force are included. The decrease in turbulence intensities by 1–2 orders of magnitude at a critical volume fraction, reported in results section, is observed even when the drag and lift corrections are included. The effect of the corrections for the drag and lift laws are briefly discussed in the “Results” section.

Direct numerical simulation. – The pressure-driven flow of a fluid with kinematic viscosity ν in a vertical channel of width h with average velocity \bar{u} is simulated using two way coupled Direct Numerical Simulations (DNS). The mean flow is in the direction of the direction of gravity. As it is mentioned earlier that the terminal velocity is smaller than the average flow velocity, gravitational effects are negligible. An Eulerian-Lagrangian method has been used. The configuration and co-ordinate system used for the simulations is shown in fig. 1. The dimensions of the channel are $4\pi h \times h \times (2\pi h/3)$ in the flow (x), wall-normal (y) and the span-wise (z) directions, where h is the channel width. Zero velocity boundary conditions are applied at the walls $y = \pm h/2$, while periodic boundary conditions are applied in the flow and the span-wise directions. The pseudo-spectral method is used to solve the Navier Stokes equation for fluid phase. Fourier transforms are used in the stream-wise and span-wise directions which are periodic, and Chebyshev transforms are used in the cross-stream direction. In order to resolve the smallest scales at $Re = 3300$, 128 Fourier modes are used in the flow direction, 64 Fourier modes in the span-wise direction and 65 Chebyshev modes in the cross-stream (y) direction. For $Re = 5600$, we use 192 Fourier modes are used in the stream-wise direction, 160 Fourier modes in the span-wise direction and 129 Chebyshev modes in the cross-stream (y). Further details are available in ref. [23]. A temporal convergence study has also been performed with different time steps between $0.003 h/\bar{u}$ and $0.01 h/\bar{u}$.

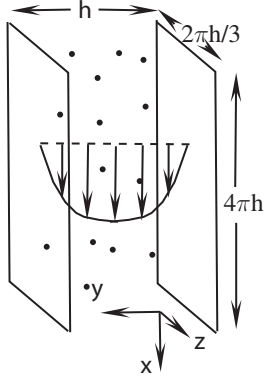


Fig. 1: Configuration and co-ordinate system used for the simulations.

In the present simulations, we have used a time step of $0.008 h/\bar{u}$ for all the simulations reported here.

The hard sphere molecular dynamics simulation procedure is used to describe the dynamics of particle phase, where the particle positions are updated based on the particle velocity, and the particle velocity is evolved using Newton's laws. The force on the particle is the sum of the gravitational force (which is negligible in the present case), the drag force (eq. (1)) and the force due to inter-particle and particle-wall collisions. The inter-particle collisions are modeled using the elastic hard-sphere model.

The lubrication forces between particles are neglected in the present analysis, since we are considering high Stokes number particles colliding in a gas. The force due to lubrication between a pair of spheres approaching each other is $F = (6\pi\mu a\Delta u/\epsilon)$, where Δu is the relative velocity, a is the particle radius and ϵ is the ratio of the gap thickness and the particle radius. In the continuum approximation, the energy dissipation due to the lubrication force ($\Delta E \sim 6\pi\mu a^2\Delta u \log(\epsilon/\epsilon_0)$) for constant relative velocity Δu diverges logarithmically as the particles approach each other. In the above expression, ϵ_0 is the scaled initial gap thickness. However, the continuum approximation breaks down when the distance between surfaces is comparable to the mean free path, about $0.1 \mu\text{m}$, or when the ratio of gap thickness and diameter is about 2×10^{-2} for $50 \mu\text{m}$ particles. The lubrication force has a log-log divergence for a free-molecular flow, and the energy dissipation is finite for the particle with high inertia. Considering the finite mean free path of the gas as λ , the initial gap thickness is h_0 , and making a conservative assumption that the particle velocity and the relative velocity scale as \bar{u} , the ratio of the energy dissipated due to lubrication in a collision and the particle kinetic energy $\frac{1}{2}m_p\bar{u}^2$ of a particle, is [24] $(\Delta E/E) = St^{-1}(d_p/h)(\log(h_0/\lambda) - 1.28)(1 + 0.15Re_p^{0.687})$. Therefore, the ratio of energy dissipation due to the lubrication and the energy of a particle is negligible in the limit of high Stokes number $St \sim 10\text{--}10^2$ and for $(d_p/h) \sim 10^{-2}$.

The particle-wall collisions are considered specular, where the particle velocity perpendicular to the wall is

reversed in a collision, while the particle velocity parallel to the wall is unchanged. The force exerted by the particle on the fluid, which is the negative of the drag force, is treated as a delta function force which is projected on the neighbouring fluid grid points using the projection on nearest neighbours (PNN) technique which was also used in [6,25]. The cell is divided into eight cuboids using three orthogonal planes parallel to the cell faces intersecting at the particle location. The fraction of the force projected onto a neighbouring grid point is the ratio of the volume of the cuboid opposite to that grid point and the total cell volume. In contrast to the more commonly used particle-in-cell (PIC) method [3,26], the particle force changes continuously as a particle crosses a cell face in the PNN method. The grid spacing in Chebyshev collocation is compressed near the wall, and the grid spacing becomes smaller than the particle size. In this case, the particle force is interpolated among the cells straddled by the particle based on the ratio of the particle surface area in each cell, as prescribed by the Faxen theorem for the velocity field. The fluid velocity at the grid points is interpolated on to the particle location using a fifth-order Lagrangian interpolation scheme; the details of the scheme and validation are explained in [23].

The initial condition for the simulation is a stationary unladen turbulent flow, where the particles are added at random locations with the same velocity as the fluid velocity. The simulation is run for 3000 integral times to reach steady state. The fluid and particle statistics are then calculated over a period of 1000 integral times. The mean fluid velocity, \bar{u}_x , is a function of the cross-stream co-ordinate y . The velocity fluctuations in the flow, cross-stream and span-wise directions are u'_x, u'_y and u'_z . The overbars are used to denote time averages, for example the mean square velocity in the flow direction is $\overline{u_x'^2}$. We have estimated standard deviation for all the results by carrying out three independent simulation runs for the same particle volume fraction but with different random initial particle locations and fluid perturbations. We found that the error is around 1–4%, comparable to the size of the symbols used.

Results. – The effect of particle loading on the mean and the mean square of the fluctuating velocities are shown in fig. 2 for channel Reynolds number 3300 and particle Stokes number 32.45. The mean and mean square velocities are symmetric about the center-line of the channel, and so each quantity is plotted in one half of the figure. The left half of fig. 2(a) shows the variation in mean velocity profiles with particle volume fraction. The mean velocity is close to the turbulent velocity profile for the unladen turbulent flow when the volume fraction is increased from 0 to 9×10^{-4} (blue). There is a distinct change in the velocity profile when the volume fraction is increased from 9×10^{-4} to 10^{-3} . The velocity profile has a higher curvature near the center and smaller gradient at the walls, and the velocity profile is closer to the parabolic profile

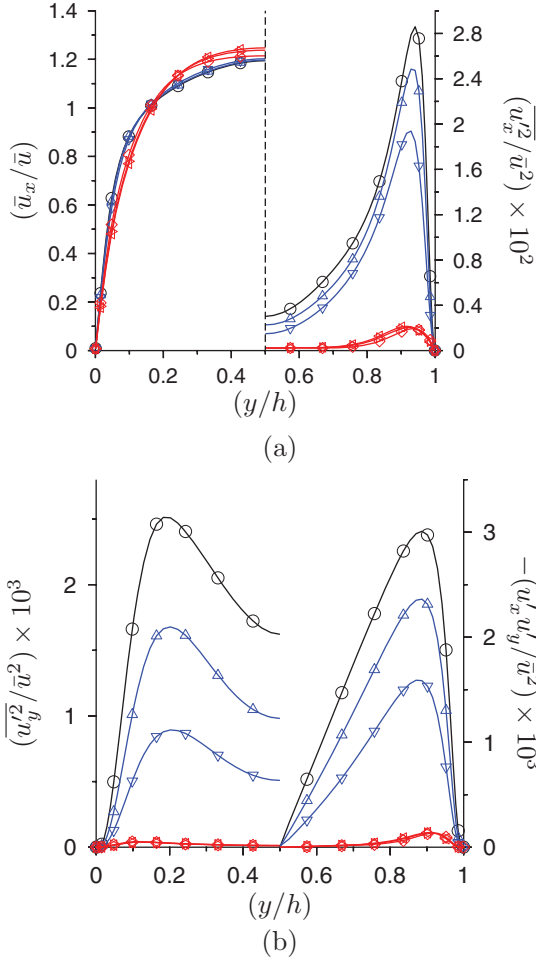


Fig. 2: In sub-figure (a), the fluid mean velocity (left half) and the stream-wise mean square fluctuating velocity (right half), and in sub-figure (b), the cross-stream mean square velocity (left half) and the correlation $\overline{u_x' u_y'}$ (right half), all suitably scaled by the powers of the average flow velocity \bar{u} , as a function of the scaled co-ordinate (y/h) , for channel Reynolds number 3300 and for average particle volume fraction 0 (\circ), 5×10^{-4} (\triangle), 9×10^{-4} (∇), 10^{-3} (\diamond), 1.1×10^{-3} (\triangleright), and 1.4×10^{-3} (\diamond). The particle Stokes number is 32.45.

for a laminar flow. When the volume fraction is further increased to 1.4×10^{-3} (red), there is little change in the velocity profile.

The change in the mean velocity profile is accompanied by a drastic reduction in the mean square velocities in all three directions. The stream-wise mean square velocity in the right half of fig. 2(a) exhibits the characteristic near-wall maximum for a turbulent flow when the volume fraction is 9×10^{-4} or less (blue lines). When the volume fraction is increased from 9×10^{-4} to 10^{-3} , there is a dramatic collapse in the mean square of the stream-wise fluctuations by one order of magnitude. Upon further increase in the volume fraction (shown in red color), there is very little change in the mean square of the fluctuating velocities. A dramatic decrease is also observed in the mean square velocities in the wall-normal direction, as shown

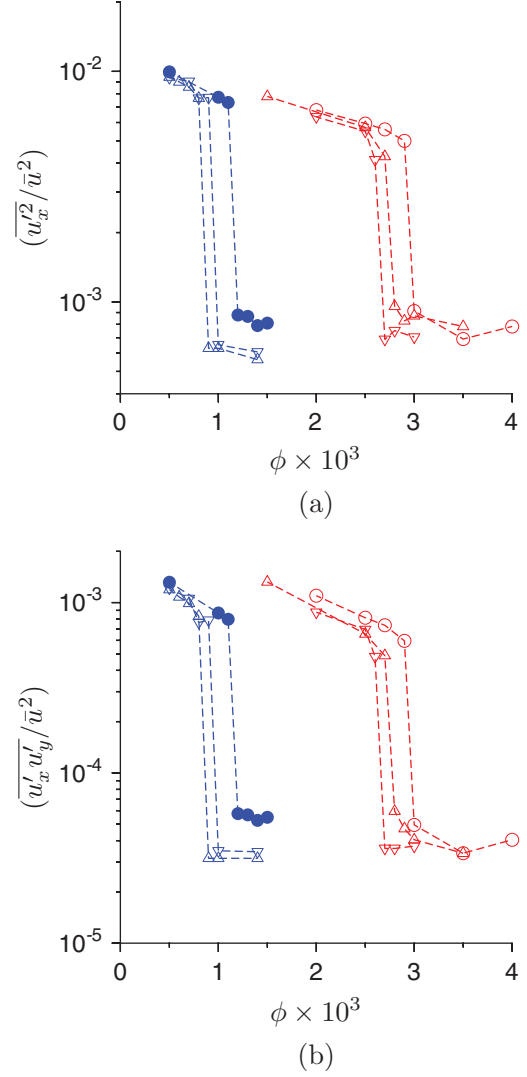


Fig. 3: The measures of the fluid fluctuating velocity $(\overline{u_x'^2}/\bar{u}^2)$ (a), $(\overline{u_x' u_y'})/\bar{u}^2$ (b) as a function of the average particle volume fraction ϕ for Stokes number 16.22 (\bullet), 64.89 (∇) and 97.34 (\triangle) for Reynolds number $Re_b = 3300$ and for Stokes number 25.11 (\circ), 50.22 (\triangle) and 75.33 (∇), for Reynolds Number $Re_b = 5600$.

in the left half of fig. 2(b). More importantly, there is also a virtual collapse in the Reynolds stress, (momentum flux due to turbulent velocity fluctuations) as shown in the right half of fig. 2(b). This implies that the suspension stress is primarily due to momentum transport by the particles for volume fraction 10^{-3} and above.

The width-averaged measures $\langle \star \rangle = \frac{2}{h} \int_0^{h/2} dy(\star)$, in stream-wise velocity fluctuations and Reynolds stress, scaled by the square of the average velocity, is shown as a function of particle average volume fraction in fig. 3. The stream-wise mean square velocity fluctuation and Reynolds stress term decreases by 1–2 orders of magnitude at critical volume fraction of the particle for both the Reynolds number and all the Stokes numbers examined here. A similar discontinuous decrease is observed in

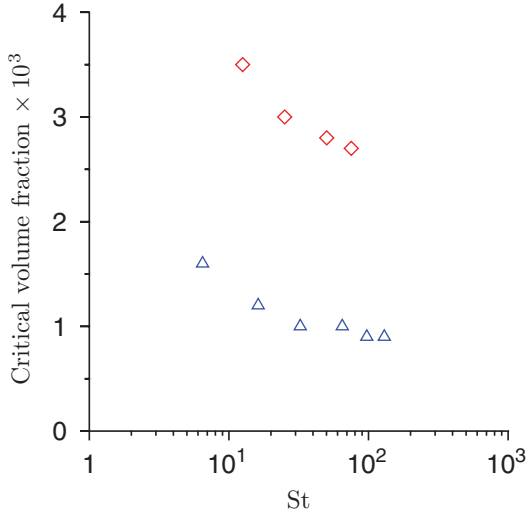


Fig. 4: The critical volume fraction for the turbulence collapse transition as a function of particle Stokes number (St) at channel Reynolds number 3300 (\triangle) and 5600 (\diamond).

all the other components of the mean square fluctuating velocities. The discontinuous transition is also observed if the Stokes drag law is used instead of the inertia corrected drag law equation (1). As explained earlier, we have incorporated the corrections due to undisturbed velocity field following [18] and also wall corrected drag and lift forces [22] to verify the effect of drag models on the prediction of turbulence collapse. It has been observed that the mean square velocities decrease by approximately 10% when the correction to the undisturbed velocity profile is added, and there is virtually no change in the mean square velocities when the drag and lift corrections are added. The turbulence intensities decrease by 1–2 orders of magnitude at a critical volume fraction even with all the above mentioned corrections, and the change in the critical volume fraction is at most 10^{-4} . This indicates that the discontinuous transition is a robust process independent of the channel Reynolds number, particle Reynolds and Stokes number and the details of the drag models used.

The critical volume fraction (ϕ_{cr}), shown as a function of the particle Stokes number in fig. 4, is independent of the Stokes number when the Stokes number is greater than about 40, and it appears to increase as the Stokes number decreases below 40 for inertia corrected drag law. When the Stokes drag law is used ϕ_{cr} is independent of the Stokes number when the Stokes number is greater than about 100. For Reynolds number 5600, the variation of critical volume fraction is not as prominent as the lower Reynolds number. The number of particles corresponding to the critical volume fractions varies between 8000 to 10000 for Reynolds number 3300 and between 20000 to 24000 for Reynolds number 5600 for different Stokes numbers.

In order to examine the mechanism of turbulence attenuation, we have calculated separately the total rates of dissipation of fluid kinetic energy, dissipation due to the

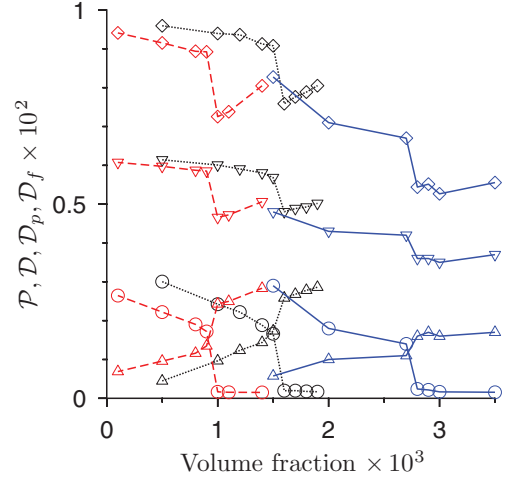


Fig. 5: The scaled total rate of dissipation of energy per unit mass \mathcal{D} (\diamond), the rate of transfer of energy per unit mass from the mean flow to the fluctuations \mathcal{P} (\circ), the rate of dissipation of energy due to the drag force exerted on the particles \mathcal{D}_p (\triangle), and the rate of dissipation of energy due to the mean shear in the fluid \mathcal{D}_f (∇) as a function of volume fraction for channel Reynolds number 3300 and particle Stokes number 6.49 (\cdots), 32.45 ($---$), and for channel Reynolds number 5600 and particle Stokes number 50.22 ($—$).

particle drag \mathcal{D}_p , and the rate of turbulent production of energy \mathcal{P} , all are calculated per unit mass of the fluid. The scaled rate of production of kinetic energy across the channel, which is also the rate of mean energy dissipation due to the turbulent velocity fluctuations at steady state is

$$\mathcal{P} = -\frac{h}{\bar{u}^3} \left\langle \overline{u'_x u'_y} \frac{d\bar{u}_x}{dy} \right\rangle_s, \quad (2)$$

where $\langle \rangle_s$ is the spatial average across the channel. The scaled rate of dissipation of energy due to the mean shear is

$$\mathcal{D}_f = \frac{\mu}{(\rho \bar{u}^3/h)} \left\langle \left(\frac{d\bar{u}_x}{dy} \right)^2 \right\rangle_s. \quad (3)$$

The scaled rate of dissipation of energy due to the drag force exerted by the particles is

$$\mathcal{D}_p = \frac{h}{\rho \bar{u}^3 V} \sum_I \overline{\mathbf{u} \cdot \mathbf{F}_I}, \quad (4)$$

where \mathbf{F}_I is the force exerted by particle I on the fluid, V is the total volume of the entire simulation cell, and the overbar is a time average. The total rate of dissipation of energy per unit mass of gas $\mathcal{D} = \mathcal{P} + \mathcal{D}_p + \mathcal{D}_f$.

The rates of total energy dissipation, turbulent production and dissipation due to the particle drag are shown as a function of the volume fraction for two different values of the channel Reynolds number and three different values of the particle Stokes number in fig. 5. It is observed that there is a significant decrease even in the total rate of dissipation of energy at the critical volume fraction. There

is a dramatic collapse in the rate of turbulent production. There is an increase in the rate of dissipation due to the particles, but this increase is only about one half of the decrease in the turbulent production. Thus, turbulence collapse is not accompanied by a compensatory increase in the energy dissipation due to the particle drag, but instead there is a decrease in the total energy dissipation rate. This indicates that the turbulence attenuation is due to a disruption of the turbulence production mechanism, rather than an increase in dissipation due to the particles.

Conclusion. – The present study has been carried out at two Reynolds numbers, 3300 and 5600 based on the channel half-width and maximum velocity. The other parameters have been varied over relatively wide ranges. Two different drag laws have been used, for Reynolds number 3300, the Stokes drag law and a modification of the Stokes law with inertial correction (eq. (1)), and 4–6 different values of the particle Stokes number have been studied for each drag. Simulations have been carried out incorporating corrections for the undisturbed velocity at the particle center, the lift force due to inertial effects, and the effect of the wall on the drag and lift forces. The turbulence collapse phenomena is also investigated at a higher Reynolds number of 5600. About 5–6 particle loadings have been considered for each Stokes number to detect turbulence collapse, and each simulation has been repeated at least 3 times resulting in a comprehensive study involving more than 500 simulations. This study has uncovered a heretofore unknown phenomenon, which is the discontinuous decrease in the turbulence intensity at a critical volume loading in a particle-gas suspension. This is in contrast to the conventional wisdom that there is a gradual decrease in the turbulence intensities as the particle loading is increased. The mechanism for turbulence modification, the disruption of the turbulent energy production in the gas phase, is different from the mechanism of increased particle dissipation which was previously considered responsible for turbulence attenuation.

The present study necessitates a re-examination of the current modeling approaches for particle-gas suspensions. The turbulence collapse at the critical volume fraction results in a decrease of about 30% in the pressure drop and energy dissipation in the simulations; this has significant implications for the design of fluidised beds and pneumatic transport processes. The decrease in the turbulent intensities by an order of magnitude will also significantly alter the particle dispersion and redistribution, coalescence and break-up processes essential for natural processes such as aerosol transport, the formation of rain-drops and particle pick-up in sand and dust storms.

The authors thank the SERB, Department of Science and Technology, Government of India, for financial support. VK would like to thank the JRD Tata Trust for supporting this research.

REFERENCES

- [1] GORE R. A. and CROWE C. T., *Int. J. Multiph. Flow*, **15** (1989) 279.
- [2] SQUIRES K. D. and EATON J. K., *Phys. Fluids A*, **3** (1991) 1169.
- [3] ELGHOBASHI S. and TRUESDELL G. C., *Phys. Fluids A*, **5** (1994) 1790.
- [4] LI Y. and MCCLAUGHLIN J. B., *Phys. Fluids*, **13** (2001) 2957.
- [5] TANAKA T. and EATON J. K., *Phys. Rev. Lett.*, **101** (2008) 114502.
- [6] VREMAN A., *J. Fluid Mech.*, **773** (2015) 103.
- [7] CAPECELATRO J., DESJARDINS O. and FOX R. O., *J. Fluid Mech.*, **845** (2018) 499.
- [8] CAPECELATRO J., DESJARDINS O. and FOX R. O., *J. Fluid Mech.*, **780** (2015) 578.
- [9] ROUSON D. W. I. and EATON J. K., *J. Fluid Mech.*, **428** (2001) 149.
- [10] DRITSELIS C. D., *Fluid Dyn. Res.*, **49** (2017) 025509.
- [11] PATEL V. C. and HEAD M. R., *J. Fluid Mech.*, **38** (1969) 181.
- [12] CARLSON D. R., WIDNALL S. E. and PEETERS M. F., *J. Fluid Mech.*, **121** (1982) 487.
- [13] SANO M. and TAMAI K., *Nat. Phys.*, **12** (2016) 249.
- [14] DRITSELIS C. D., *Fluid Dyn. Res.*, **48** (2016) 015507.
- [15] BALACHANDAR S., *Int. J. Multiph. Flow*, **35** (2009) 801.
- [16] BALACHANDAR S. and EATON J. K., *Annu. Rev. Fluid Mech.*, **42** (2010) 111.
- [17] MEHRABADI M., HORWITZ J., SUBRAMANIAM S. and MANI A., *J. Fluid Mech.*, **850** (2018) 336.
- [18] ESMAILY M. and HORWITZ J., *J. Comput. Phys.*, **375** (2018) 960.
- [19] SAFFMAN P., *J. Fluid Mech.*, **22** (1965) 385.
- [20] ZHANG H. and AHMADI G., *J. Fluid Mech.*, **406** (2000) 55.
- [21] WANG Q., SQUIRES K., CHEN M. and MCCLAUGHLIN J., *Int. J. Multiph. Flow*, **23** (1997) 749.
- [22] ZENG L., NAJJAR F., BALACHANDAR S. and FISCHER P., *Phys. Fluids*, **21** (2009) 033302.
- [23] GOSWAMI P. S. and KUMARAN V., *J. Fluid Mech.*, **687** (2011) 1.
- [24] SUNDARARAJAKUMAR R. R. and KOCH D. L., *J. Fluid Mech.*, **313** (1996) 283.
- [25] EATON J. K., *Int. J. Multiph. Flow*, **35** (2009) 792.
- [26] SQUIRES K. D. and EATON J. K., *Phys. Fluids A: Fluid Dyn.*, **2** (1990) 1191.